WATER RESOURCES RESEARCH, VOL. 27, NO. 10, PAGES 2707-2718, OCTOBER 1991

The Second Las Cruces Trench Experiment: Experimental Results and Two-Dimensional Flow Predictions

R. G. HILLS

Mechanical Engineering Department, New Mexico State University, Las Cruces

P. J. WIERENGA AND D. B. HUDSON

Department of Soil and Water Science, University of Arizona, Tucson

M. R. KIRKLAND

Mechanical Engineering Department, New Mexico State University, Las Cruces

As part of a comprehensive field study designed to provide data to test stochastic and deterministic models of water flow and contaminant transport in the vadose zone, several trench experiments were performed in the semiarid region of southern New Mexico. The first trench experiment is discussed by Wierenga et al. (this issue). During the second trench experiment, a 1.2 m wide by 12 m long area on the north side of and parallel to a 26.4 m long by 4.8 m wide by 6 m deep trench was irrigated with water containing tracers using a carefully controlled drip irrigation system. The irrigated area was heavily instrumented with tensiometers and neutron probe access tubes to monitor water movement, and with suction samplers to monitor solute transport. Water containing tritium and bromide was applied during the first 11.5 days of the study. Thereafter, water was applied without tracers for an additional 64 days. Both water movement and tracer movement were monitored in the subsoil during infiltration and redistribution. The experimental results indicate that water and bromide moved fairly uniformly during infiltration and the bromide moved ahead of the tritium due to anion exclusion during redistribution. Comparisons between measurements and predictions made with a two-dimensional model show qualitative agreement for two of the three water content measurement planes. Model predictions of tritium and bromide transport were not as satisfactory. Measurements of both tritium and bromide show localized areas of high relative concentrations and a large downward motion of bromide relative to tritium during redistribution. While the simple deterministic model does show larger downward motions for bromide than for tritium during redistribution, it does not predict the high concentrations of solute observed during infiltration, nor can it predict the heterogeneous behavior observed for tritium during infiltration and for bromide during redistribution.

INTRODUCTION

Prediction of water flow and chemical transport through unsaturated soils generally requires the use of numerical models. Examples of such models include those of *Ababou and Gelhar* [1988], *Allen and Murphy* [1986], *Hills et al.* [1989*a*, *b*], *Huyakorn et al.* [1986*a*, *b*, 1989], *Huyakorn and Pinder* [1983], *Kaluarachchi and Parker* [1987], and *van Genuchten* [1982, 1983]. Most of these models allow spatially variable soils to be modeled deterministically while others allow the soils to be modeled stochastically. While these models provide various levels of theoretical sophistication, the advantages of one model over another cannot be fully demonstrated under actual field conditions until adequate field data become available.

The field experiment presented here is one of several experiments being performed at the Las Cruces Trench Site to provide the data for testing deterministic and stochastic flow and transport models. Other experiments performed at this site include site characterization experiments [*Wierenga et al.*, 1988, 1989, this issue], several field scale lysimeter experiments [*Wierenga et al.*, 1988; *Hills et al.*, 1989*b*], and an earlier infiltration experiment [*Wierenga et al.*, this issue]. Here we discuss the experimental techniques used during the second trench experiment. Field observations of water, tritium, and bromide movement during infiltration and redistribution are presented. In addition, comparisons are made between the field observations and model predictions using simple two-dimensional deterministic numerical models for water flow and solute transport. These simple models provide base cases against which more sophisticated deterministic and stochastic models can be tested in the future.

Paper number 91WR01538.
0043-1397/91/91WR-01538$05.00

METHODS, MATERIALS, AND THEORY

Site Description and Characterization

A 26.4 m long by 4.8 m wide by 6.0 m deep trench was constructed in the undisturbed soil at the Las Cruces Trench Site to provide horizontal access to adjacent irrigated plots and to provide soil samples for soil characterization. The physical description, the soil morphology, and the site characterization experiments are discussed by *Wierenga et al.* [this issue] with additional information on site characterization and parameter estimation procedures given by *Wierenga et al.* [1989].

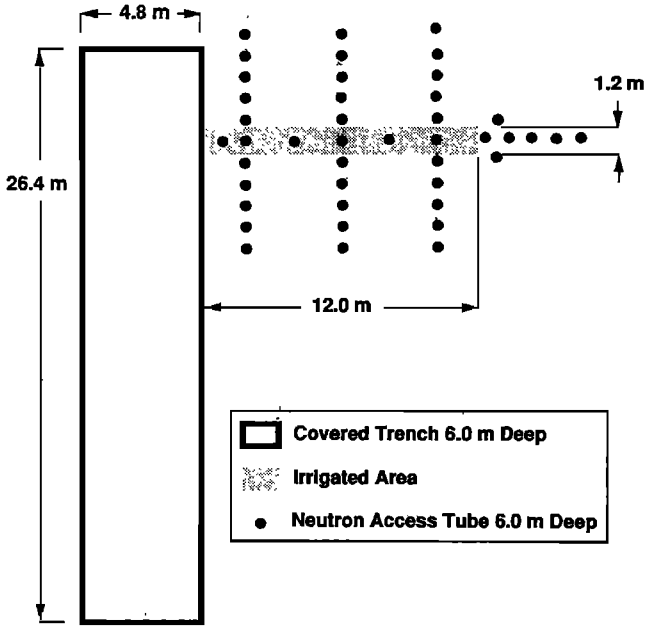

Fig. 1. Plan view of the trench face, the irrigated area, and the neutron access tubes.

Monitoring Water Flow and Solute Transport

Forty-three neutron access tubes, each 6 m deep, were installed in and around the 1.2 m by 12 m area adjacent to the north side of the trench. The positions of the access tubes with respect to the trench and the irrigated area are shown in Figure 1. The neutron probe was calibrated at the experimental site by gravimetric sampling [*Wierenga et al.*, 1988]. Neutron probe readings were taken every 4 to 5 days during irrigation but less often during redistribution. Readings were taken at 0.25 m depth increments with a CPN 503 DR neutron probe (CPN Corporation, Martinez, California).

Tensiometers were installed through the trench face such that the porous cup of each tensiometer was inserted 50 cm into the formation at an angle of 10° from the horizontal. The locations of the tensiometers are shown in Figure 2. The exposed ends of the tensiometers extend approximately 15 cm into the trench. Pressures were measured through a septum stopper at the exposed end of each tensiometer using a hand-held pressure transducer (Soil Measurement Systems, Tucson, Arizona). The tensiometer measurements were taken every 2 to 3 days during irrigation and less often during redistribution.

Soil solution samplers were also installed in a grid pattern through the trench wall in the same manner as the tensiometers (see Figure 2). Once the water front had reached the samplers, a constant vacuum of approximately 200 mbar was applied to the samplers to collect soil solution samples. Samples were collected every 2 to 3 days during irrigation and less often during redistribution. When the wetting front had passed a row of tensiometers, the center three tensiometers were converted to solute samplers to provide a denser sampling grid. These samplers are denoted as sampler/tensiometers in Figure 2.

Water Application

Water from a nearby irrigation well was applied to the 1.2 m by 12 m area through a closely spaced grid of drip emitters. A total of 40 parallel irrigation lines were used. Each line was 1.2 long and contained four drippers. Alternating lines were connected to two separate header pipes, which in turn were connected to the water supply system. Water was applied twice a day (once a day to each header line) resulting in an average surface flux of 0.43 cm/d over the irrigated area. The irrigated area and surrounding area were covered by a reinforced 36-mil chlorinated polyethelene pond liner to inhibit evaporation from the surface and to prevent infiltration of rain water.

Water application to the 1.2 m by 12 m area was started on August 8, 1988. It was stopped 75.5 days later after 4721 L of water had been applied at a uniform rate. Tritium and bromide tracers were applied in the irrigation water during the first 11.5 days of irrigation. A total of 71.95 mCi of tritium was added to the first 719.5 L of water, resulting in an applied tritium concentration of 0.1 mCi/L. Bromide was applied at a concentration of 939 mg/L.

Modeling Water Flow

To help evaluate the completeness of the data set for deterministic modeling applications, simple two-dimensional numerical simulations of water flow and solute transport were performed. The intent of these simulations was to provide a base case against which more sophisticated deterministic and stochastic models can be tested in the future. Richards' equation for two-dimensional water flow with isotropic hydraulic conductivity is given by

$$\frac{\partial \theta}{\partial t} + \frac{\partial}{\partial x}\left(K\frac{\partial h}{\partial x}\right) + \frac{\partial}{\partial z}\left(K + K\frac{\partial h}{\partial z}\right) = 0 \qquad (1)$$

where θ is the volumetric water content, K is the hydraulic conductivity, h is the tension, t is time, x is the horizontal position, and z is the vertical position measured downward. Writing (1) in terms of water content gives

$$\frac{\partial \theta}{\partial t} - \frac{\partial}{\partial x}\left(D\frac{\partial \theta}{\partial x}\right) - \frac{\partial}{\partial z}\left(D\frac{\partial \theta}{\partial z} - K\right) = 0 \qquad (2)$$

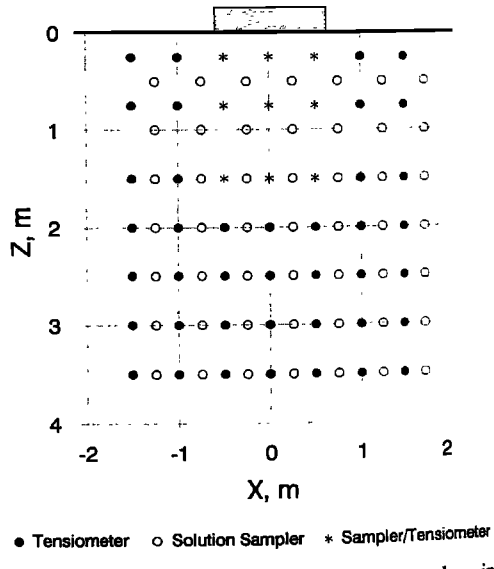

Fig. 2. Location of tensiometers and solute samplers in trench wall.

where D is defined by

$$D \equiv -\frac{K}{d\theta/dh}. \tag{3}$$

While (2) is not valid across soil layers, it can be applied to a uniform soil. Here we use a two-dimensional extension of the one-dimensional algorithm developed by *Hills et al.* [1989*a*]. This extension is based on the alternating direction implicit method and is used to model water flow in a uniform soil. The details of this algorithm are presented in the appendix. We will present an extension of this algorithm to heterogeneous soils in a later paper.

The initial and boundary conditions on water content are taken to be

$$\theta(x, z, 0) = \theta_{\text{init}}(z) = \theta(h_{\text{init}}(z)), \tag{4a}$$

$$\left(K - D\frac{\partial\theta}{\partial z}\right)\bigg|_{z=0} = 0.43 \text{ cm/d} \tag{4b}$$

$$-0.61 \text{ m} \le x \le 0.61 \text{ m}; \; t \le 75.5 \text{ days};$$

$$\left(K - D\frac{\partial\theta}{\partial z}\right)\bigg|_{z=0} = 0 \qquad \text{otherwise}$$

$$\left(K - D\frac{\partial\theta}{\partial z}\right)\bigg|_{z=b} = 0.0, \tag{4c}$$

$$D\frac{\partial\theta}{\partial x}\bigg|_{x=-a} = 0.0, \tag{4d}$$

$$D\frac{\partial\theta}{\partial x}\bigg|_{x=a} = 0.0, \tag{4e}$$

where a and b are sufficiently large, and the initial water contents sufficiently small so that significant water movement does not occur normal to these boundaries during the simulation. Values of $a = 5.0$ m and $b = 6.0$ m were adequate for 300 days of simulation. Van Genuchten's water retention and unsaturated hydraulic conductivity models [*van Genuchten*, 1980] are used for the present simulations:

$$S_e = \frac{\theta - \theta_r}{\theta_s - \theta_r} = \frac{1}{[1 + (\alpha h)^n]^m}, \tag{5}$$

$$m = 1 - \frac{1}{n}, \tag{6}$$

where θ, θ_r, and θ_s are the volumetric water content, residual water content, and saturated water content, respectively, α and n are parameters that affect the shape of the retention curve, and h is tension. Given estimates of the parameters in (5) and an effective value for the saturated hydraulic conductivity, the unsaturated hydraulic conductivity can be modeled by [*van Genuchten*, 1980]

$$K = K_s S_e^{1/2}[1 - (1 - S_e^{1/m})^m]^2. \tag{7}$$

Estimates for the parameters that appear in (5) and (7) are discussed by *Wierenga et al.* [this issue] for both a uniform and a layered soil model for the Las Cruces Trench Site.

TABLE 1. Initial Tensions Used for the Numerical Simulation

Depth, cm	h, cm H_2O
25	143.9
75	170.2
100	249.3
150	215.5
210	28,860
285	36,980
360	47,090
435	48,020
510	53,300
585	56,330
660	64,940

For $z \le 1.5$ m, tensiometers measurements were used; for $z > 1.5$ m, psychrometer measurements were used.

Here we use the uniform soil model parameters. These are given by

$$\theta_s = 0.3209, \qquad \theta_r = 0.0828, \qquad \alpha = 0.05501 \text{ cm}^{-1},$$

$$n = 1.5093, \qquad K_s = 270.1 \text{ cm/d}$$

The initial water content $\theta_{\text{init}}(z)$ for the model is determined from the water retention model and observed initial tensions. The upper 1.5 m of the soil was initially wet enough to be in the tensiometer range ($h < 500$ cm). These high near-surface water contents were due to heavy rainfall in the weeks prior to covering the experimental plot. To obtain a depth dependent model for initial tension, averages of all the tensions obtained from tensiometers at similar depths down to 1.5 m were taken. The tensions from tensiometers installed through the trench face (Figure 2) and from tensiometers installed vertically through the surface of the irrigated area were used to obtain the averages. Specifically, the readings from eight tensiometers at 0.25 m, five tensiometers at 0.75 m, four tensiometers at 1.0 m, and six tensiometers at 1.5 m depth were averaged. Since only two good readings were obtained at a depth of 0.5 m, an average value for this depth was not included in the initial tension model. These measurements were taken on day 1, which was the first day that readings were available after the plot was fully covered. The initial tensions were too high to be in the tensiometer range for depths greater than 1.5 m. Initial field tensions for depths greater than 1.5 m were obtained from soil samples using a thermocouple psychrometer (Decagon Devices, Inc., Pullman, Washington). Seven samples were taken from each of seven depths (ranging from 2.1 to 6.6 m) and the resulting initial tensions averaged. These samples were collected during the installation of the neutron probe access tubes along the centerline of the irrigated area. The resulting average tension versus depth data are shown in Table 1. For simulation purposes, an initial tension of 143.9 cm H_2O was used for depths less than 25 cm. Linear interpolation was used to estimate the initial tensions at intermediate depths.

Solute Transport

To model the transport of tritium and bromide, the convection/dispersion equation is used with the assumption that the dispersivity is homogeneous and isotropic and that the solute is nonreactive and nondecaying. Neglecting the radioactive decay of tritium results in only a 1% error in concen-

tration on day 71 and a 4% error on day 277 due to tritium's half-life of 12.26 years. The governing partial differential equation is given by

$$\frac{\partial}{\partial t}(R\theta c) = \frac{\partial}{\partial x}\left(\theta D_s \frac{\partial c}{\partial x} - q_x c\right) + \frac{\partial}{\partial z}\left(\theta D_s \frac{\partial c}{\partial z} - q_z c\right) \quad (8)$$

where R is the retardation factor, D_s is the dispersion coefficient, q_x and q_z are the Darcian fluxes and x and z are coordinate directions. A normalized or relative concentration is used for c where the normalization constant is the average concentration applied during the first 11.5 days of the experiment. The normalized or relative concentration for the solute applied at the surface is thus unity. The x and z components of the Darcian fluxes are given by

$$q_x = K\frac{\partial h}{\partial x} = -D\frac{\partial \theta}{\partial x} \quad (9a)$$

$$q_z = K + K\frac{\partial h}{\partial z} = K - D\frac{\partial \theta}{\partial z} \quad (9b)$$

where h represents tension. The dispersion coefficient, D_s (the subscript s is used to distinguish the dispersion coefficient from the hydraulic diffusivity, D), is given by

$$\theta D_s = \theta D_m + \varepsilon|\mathbf{q}| \quad (10)$$

where D_m is the molecular dispersion coefficient, ε is the dispersivity, and $|\mathbf{q}|$ is the magnitude of the Darcian flux. Here the dispersivity and molecular dispersion coefficient are assumed to be homogeneous and isotropic, leading to a dispersion coefficient that is a scalar. Field dispersivity values typically range up to 10 cm or more [*Nielsen et al.*, 1986]. Since the dispersivity has not been determined for the trench experiment, we somewhat arbitrarily choose $\varepsilon = 5$ cm. The molecular diffusion D_m was assumed to be 1.0 cm^2/d. The relatively low value for ε is typical of the soils at the Las Cruces Trench Site and results in transport that is dominated by convection rather than dispersion. Retardation factors of 1.0 for tritium and 0.84 for bromide were used. The low retardation factor for bromide is based on studies with laboratory columns and field lysimeters filled with topsoil removed from the area surrounding the trench site. No attempt was made to "calibrate" the model by choosing other values for the dispersivity or the retardation factor.

The initial concentration was taken to be zero. Zero fluxes on the lateral and lower boundaries and a constant flux on the upper boundary were specified. The initial and boundary conditions for the relative concentration $c(x, z, t)$ are given by

$$c(x, z, 0) = 0.0 \quad (11a)$$

$$\left(q_z c - \theta D_s \frac{\partial c}{\partial z}\right)\Bigg|_{z=0} = 0.43 \text{ cm/d} \quad (11b)$$

$$-0.61 \text{ m} \le x \le 0.61 \text{ m};\ t \le 11.5 \text{ days};$$

$$\left(q_z c - \theta D_s \frac{\partial c}{\partial z}\right)\Bigg|_{z=0} = 0 \quad \text{otherwise.}$$

$$\left(q_z c - \theta D_s \frac{\partial c}{\partial z}\right)\Bigg|_{z=b} = 0.0, \quad (11c)$$

$$\left(q_x c - \theta D_s \frac{\partial c}{\partial x}\right)\Bigg|_{x=-a} = 0.0, \quad (11d)$$

$$\left(q_x c - \theta D_s \frac{\partial c}{\partial x}\right)\Bigg|_{x=a} = 0.0. \quad (11e)$$

Again, the a and b must be taken to be sufficiently large so that the wetting and solute fronts do not interact with the boundaries during the numerical simulation. Note that the normalized concentration of the solute applied to the surface is unity and dimensionless. Thus the right-hand side of (11*b*) has the units of centimeters per day.

The solutions to (10) and (11) were approximated through the use of an alternating direction implicit finite difference algorithm. The convective terms were handled explicitly using center differences. The grid size was taken to be sufficiently small so that the convective terms did not lead to stability problems. During each time step, Richards' equation was solved, the water contents and Darcian fluxes were evaluated, and then the transport equation was solved. Details of the finite difference approximations are provided in the appendix.

Implementation of the Numerical Algorithms

The water flow and transport algorithms were implemented in VAX FORTRAN using double-precision arithmetic. The water flow algorithm was validated by comparing algorithm predictions against those obtained from other one-dimensional water content and head-based water flow algorithms [*Hills et al.*, 1989*a*]. Separate horizontal and vertical water flow numerical experiments were performed to validate the two-dimensional algorithm along both coordinate directions. Mass balance errors were also calculated and found to be within machine precision.

The transport algorithm was validated against one-dimensional analytical solutions of the transport equation (in both directions) using various boundary and initial conditions. The solute mass balance errors were calculated and also found to be within machine precision.

A 6 m deep by 10.1666 m wide model domain was used. Symmetry was assumed along the vertical centerline of the irrigated area to reduce the computational domain to a 6 m deep by 5.0833 m wide area. The grid and time step sizes used for all numerical simulations were $\Delta x = 0.050833$ m, $\Delta y = 0.05$ m and $\Delta t = 0.5$ days. A value of 0.050833 for Δx was used to insure that the irrigation width (1.22 m) could be represented by an integer number of Δx intervals. To check convergence and the effect of numerical diffusion/dispersion, contour plots of water flow and solute transport on days 71 and 277 were compared to those obtained when the time and spatial step sizes were halved. The differences between the fine grid and coarse grid contours were found to be insignificant.

Here we use contour plots to compare model predictions to field observations. Since the resulting contours can be very sensitive to density of the sampling grid used to generate the contours, model predictions were sampled on a

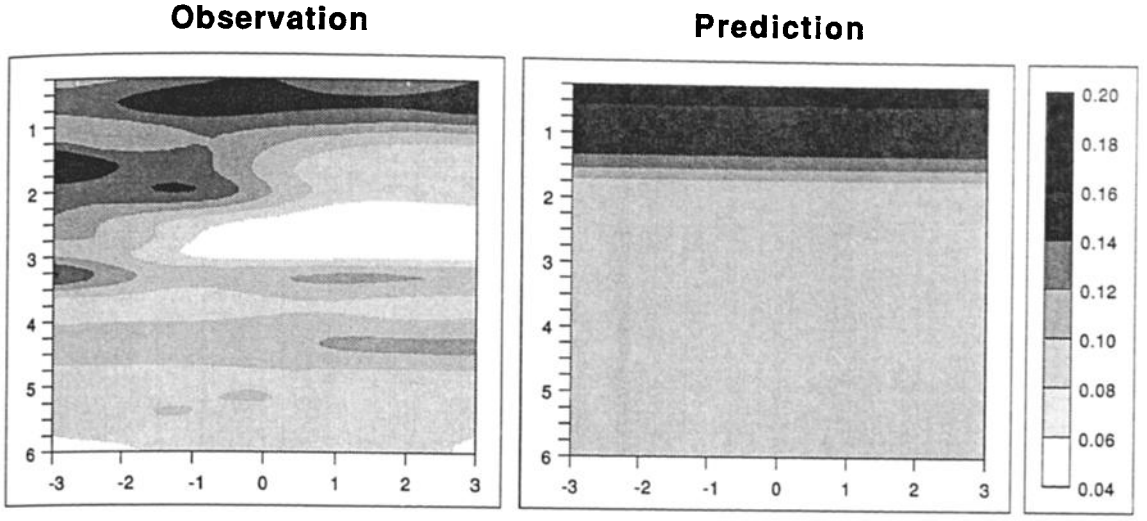

Fig. 3. Observed and modeled initial water contents: $y = 2$ m.

grid with the same density as the corresponding field observations. This grid is much coarser than the finite difference grid (the full finite difference grid was used to check convergence). For example, the model predictions were sampled on a grid with a horizontal increment of 1 m and a vertical increment of 0.25 m. This is the same sampling grid as was used for the neutron probe measurements. A 0.25 m by 0.25 m contour grid was used for the solute predictions. Due to the irregular nature of the measurement sampling grid (see Figure 2), weighted averages of all measurements made within two grid cells of a grid node were used to estimate the nodal value of concentration. Inverse distance squared weighting was used. The axis tick marks shown in the figures represent the intersection of the contour grid with the vertical and horizontal axes. Once the nodal values for water content and relative concentration were determined, WingZ (Informix Software, Inc., Lenexa, Kansas) was used to generate the contour plots. WingZ is a Macintosh-based spreadsheet and uses B splines to generate smooth contour surfaces.

DISCUSSION OF RESULTS

Figures 3 and 4 show the water contents as measured in vertical planes 2 m, 6 m, and 10 m from the trench wall (see Figure 1) on day 1. The vertical axis in each contour plot represents depth in meters and the horizontal axis represents horizontal distance in meters from the irrigation area centerline. Contours were not shown for depths less than 0.25 m since no measurements were made at these depths. To facilitate the comparison, the initial water contents for the model are presented together with the observed water contents for the $y = 2$ m plane. The $y = 2$ m plane is closest to the plane of solute samplers ($y = 0.5$ m) and to the plane from which the soil samples were taken for characterization ($y = -0.5$ m). Day 1 represents the first day that measurements were taken after the plot was covered. As a result of significant rainfall and the lack of a cover on previous days, the day 1 observations represent the best estimate of the initial conditions that existed prior to the controlled application of the water and solute. Figures 3 and 4 illustrate the

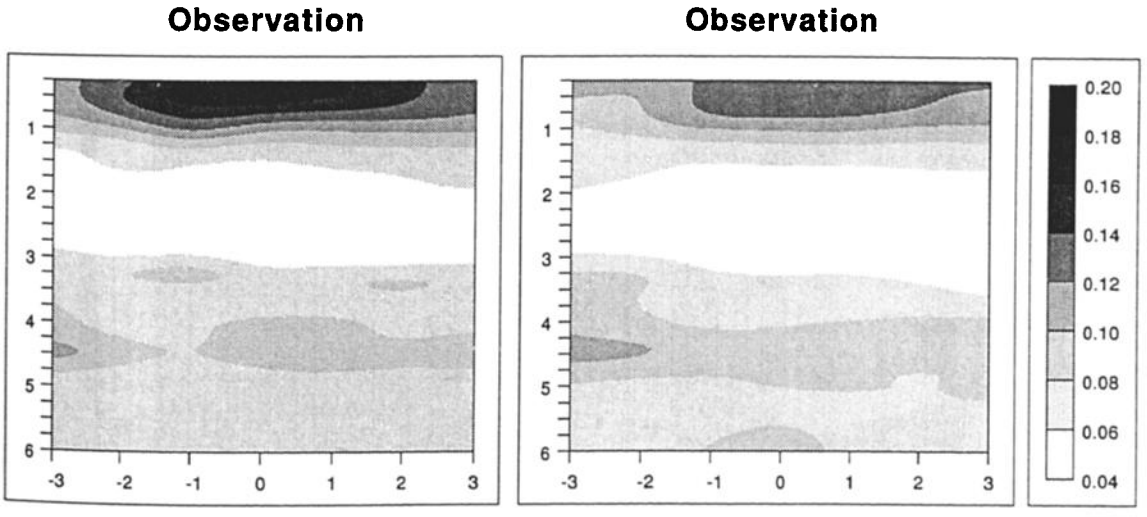

Fig. 4. Observed initial water contents: (left) $y = 6$ m and (right) $y = 10$ m.

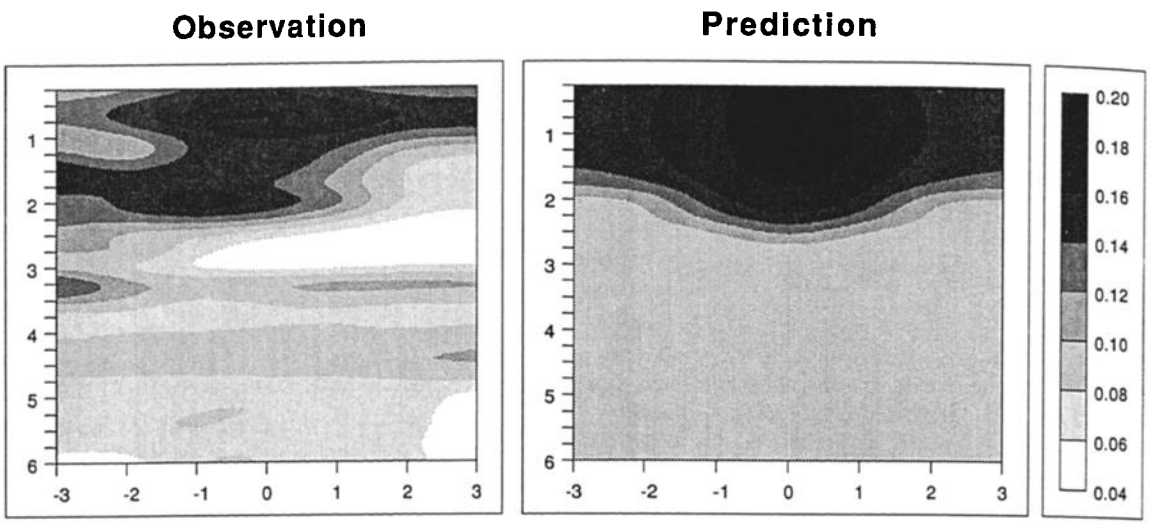

Fig. 5. Observed and predicted water contents on day 71: y = 2 m.

presence of spatial variability in the observed water contents with strong indications of layering. The day 1 volumetric water contents range from less than 0.04 cm^3/cm^3 to greater than 0.16 cm^3/cm^3 with wetter conditions occurring near the surface at y = 6 m. In contrast, the initial water content distribution for the finite difference simulation (see Figure 3), which is based on a simple depth dependent tension model (Table 1), shows no variation in the y direction. Also, the high initial water contents (>0.08 cm^3/cm^3 throughout and >0.16 cm^3/cm^3 near the surface) suggest that the uniform soil retention model overpredicts the water contents at the initial tensions used, especially at intermediate depths where the observed initial water contents range from 0.04 to 0.08 cm^3/cm^3.

Comparisons between observed and predicted water contents and the changes in water contents on day 71 for the y = 2 m plane are presented in Figures 5 and 6, respectively. The observed changes in water content are the differences between the water contents measured on day 71 and those measured on day 1. The predicted changes in water content are the differences between the predicted water contents on day 71 and the initial water contents for the model. The change in water contents are plotted because they better illustrate movement of water than do absolute water contents. Also, the observed changes show less effect of spatial variability and are somewhat easier to interpret. The water content changes for the observation planes at y = 6 m and 10 m are shown in Figure 7. As Figures 6 and 7 illustrate, the water moves in a fairly uniform fashion for all three planes during the first 71 days of infiltration. More spreading occurs in the y = 6 m plane than in the other planes. After 71 days of water application, the contours suggest that the leading edge of the wetting front has generally moved downward to a depth of 2–2.5 m while it has moved laterally from each edge of the irrigated zone by 1–2 m. Overall, the leading edges of the predicted water content differences show average vertical movements that agree qualitatively with the observations made in the three planes. Comparisons of the predicted and observed lateral spreading show less agreement and show more sensitivity to the effects of spatial variability. The large degree of lateral spreading demonstrated in the numerical predictions (Figure 6) suggests that

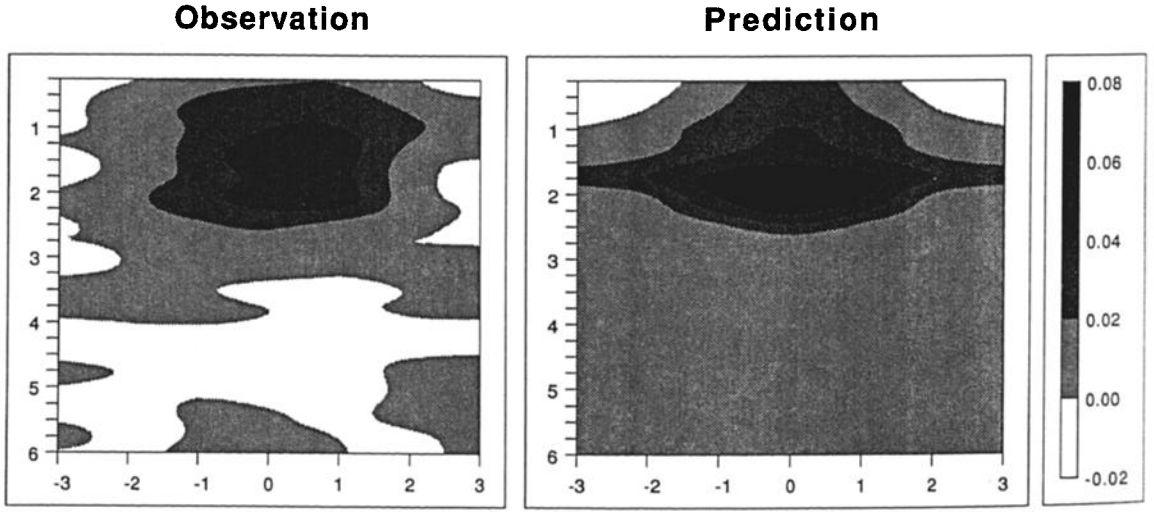

Fig. 6. Changes in observed and predicted water contents on day 71: y = 2 m.

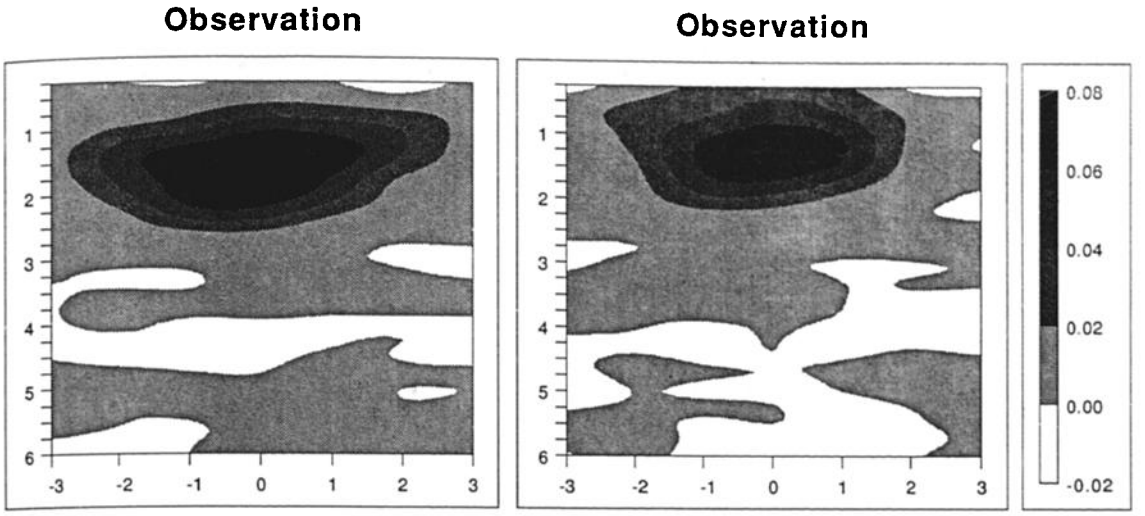

Fig. 7. Changes in observed water contents on day 71: (left) $y = 6$ m and (right) $y = 10$ m.

the tension gradient rather than gravity is the dominant driving force at the low flow rates present. There is little movement of water during the first 71 days at depths greater than 3 m. However, very small differences in the measured water contents can result in negative changes in the water contents at these depths. These small changes may be due to water movement or simply due to random error in the neutron probe measurements. Most of the spatial variation in the change in water contents shown below the wetting front in Figures 6 and 7 is a result of these very small differences.

The observed and predicted relative tritium and bromide concentrations on day 71 in the $y = 0.5$ m plane are shown in Figures 8 and 9. Note that the tritium and bromide fronts lag far behind the water front (note that different scales are used for Figures 6 and 8). Displacement of the initial water in the soil profile causes this lag. Also note that the predicted bromide front moves slightly faster than the predicted tritium front (Figures 8 and 9). This is a result of the lower retardation factor due to anion exclusion for bromide. In contrast to the day 71 model predictions, this effect is not readily apparent in the day 71 observations. The 0.05 contours for the model predictions and the field observations for both tritium and bromide tend to show qualitatively similar downward and lateral motions of the solute front. However, the observed relative peak concentration of tritium is much higher than the predicted peak concentrations at 1 m depth and 0.5 m to the right of the centerline. The observed day 71 relative bromide concentrations also are higher than model predictions at 1 m depth but do not display as strong a net horizontal motion.

Figures 10 and 11 show the observed and predicted changes in water contents for day 276. Since water application stopped on day 75.5, day 276 represents 200.5 days of redistribution. Note that the observations show an overall downward movement of water with a rightward net motion in water content for the $y = 2$ m plane. This net horizontal motion is greater after 200 days of redistribution for the $y = 2$ m plane than after the 71 days of infiltration. The observations show that the model underpredicts the maximum depth of the leading edge of the wetting front (defined here as the 0.02 contour) for the $y = 2$ m case and overpredicts the wetting front location for the $y = 10$ m case for day 276. The comparison improves for the $y = 6$ m case. However, it is clear that the deterministic model used here cannot accurately predict point values for water content due to spatial variation in field hydraulic properties since this variation is not accounted for in the model.

The relative tritium and bromide concentration profiles for day 277 (no solute samples were taken on day 276) are shown

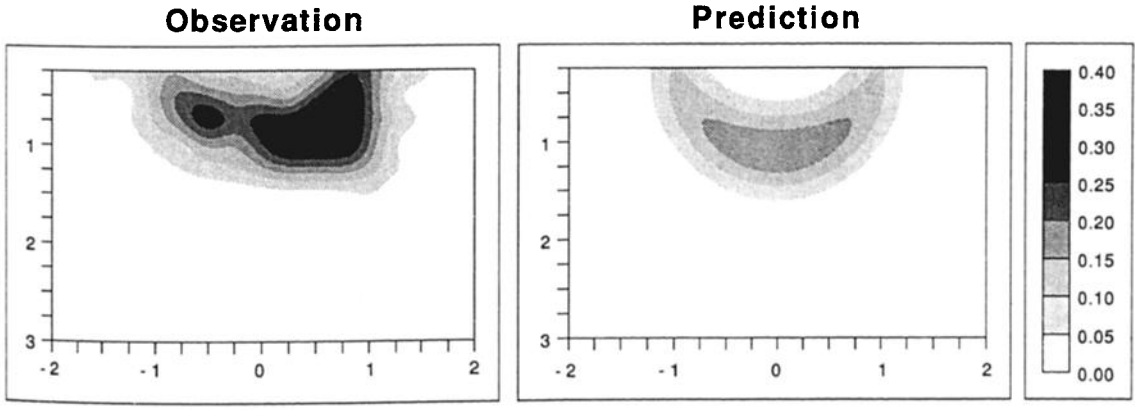

Fig. 8. Observed and predicted relative tritium concentrations on day 71: $y = 0.5$ m.

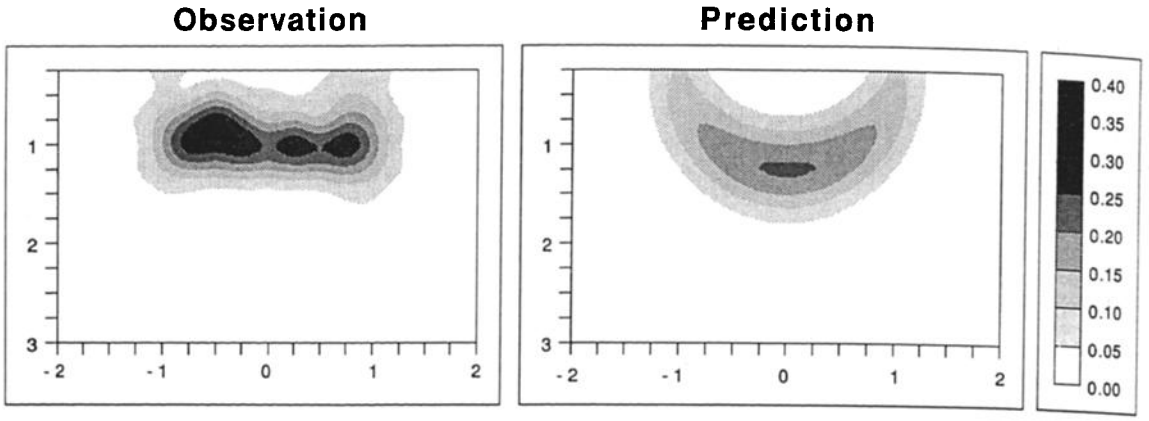

Fig. 9. Observed and predicted relative bromide concentrations on day 71: $y = 0.5$ m.

in Figures 12 and 13. Comparing Figures 8 and 9 with Figures 12 and 13 suggests that tritium moves little during the 201.5 days of redistribution. In contrast, the bromide shows significant downward and rightward motion during the same period. A possible explanation for this contrasting behavior is that the effect of anion exclusion forces the bromide closer to the leading edge of the water front where most of the redistribution occurs. As a result, the transport of bromide appears to be correlated to the higher day 276 water content changes and the lower day 1 water contents which exist toward the right as illustrated in Figures 10 and 3. The model predictions show a downward motion of tritium during redistribution, suggesting an overprediction of water movement due to gravity at depths around 1 m or suggesting that some other physical mechanism is present in the soil which is retarding the motion of tritium. Comparisons between model predictions and the measured relative bromide concentrations show similar depths of penetration for the tracer fronts but significant differences in lateral motion. Bromide shows a larger net movement to the right than does tritium after 201.5 days of redistribution. This is in contrast to the day 71 results. However, it should be noted that Figure 13 is somewhat incomplete in that many solution samplers failed to operate to the left of $x = 0.5$ m because the soil water content was too low.

Considering the simplistic nature of the water flow model, the model was surprisingly good at predicting water flow during the 75 days of infiltration for all three planes and during the subsequent 200 days of redistribution for two of the three neutron probe measurement planes. However, there were large discrepancies between prediction and observation for the $y = 2$ m plane during redistribution due to lateral heterogeneities in the soil. These heterogeneities were apparent in both the day 1 and day 276 observations.

Bromide showed a similar nonhomogeneous behavior during redistribution. This is not surprising considering that the solute sampling plane ($y = 0.5$ m) is close to the $y = 2$ m neutron probe plane. The significant differences in the observed motion of tritium and bromide are surprising. Although they were applied together, tritium showed a stronger nonhomogeneous motion during infiltration but little motion during redistribution. In contrast, bromide showed a fairly homogeneous motion during infiltration but a highly nonhomogeneous motion during redistribution. The simple uniform soil transport model cannot predict this heterogeneous behavior.

CONCLUSIONS

To further develop a data base on water flow and solute transport in spatially variable soils for model validation,

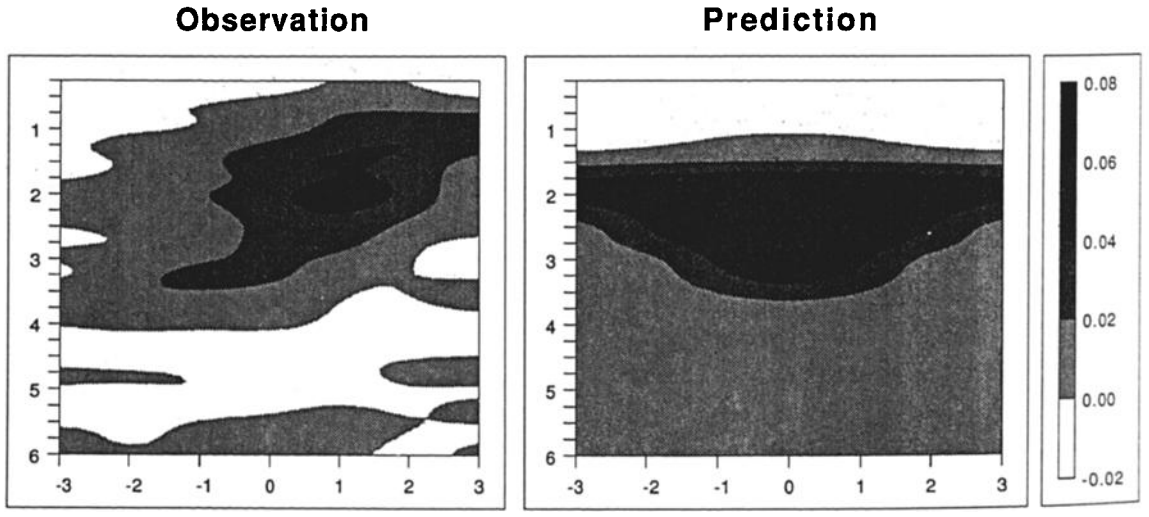

Fig. 10. Changes in observed and predicted water contents on day 276: $y = 2$ m.

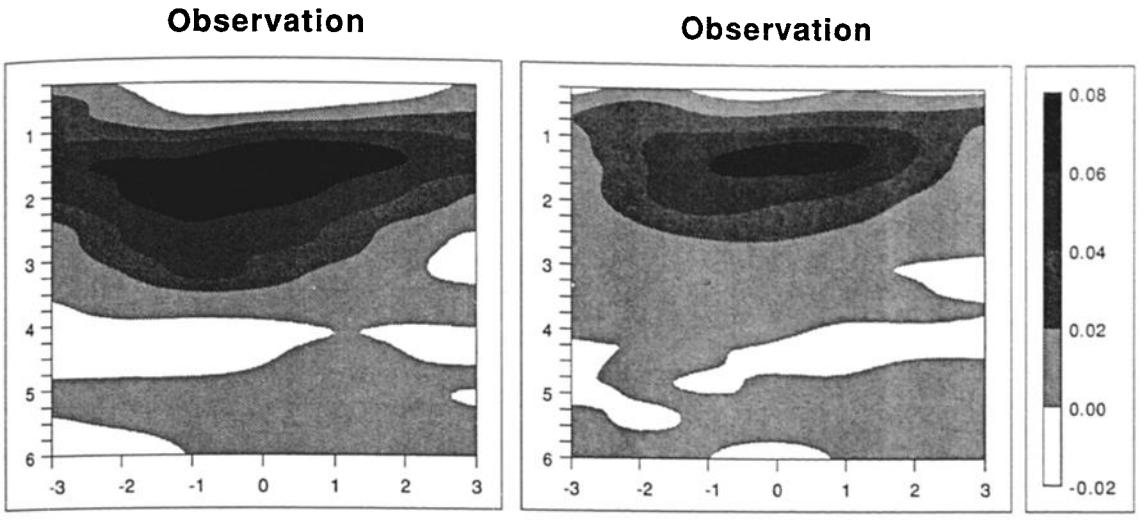

Fig. 11. Changes in observed water contents on day 276: (left) y = 6 m and (right) y = 10 m.

trench experiment was performed at an arid site in southern New Mexico. An experimental plot was irrigated in a controlled fashion and the movement of water and several tracers was monitored over several two-dimensional grids through the use of neutron probes, tensiometers, and solution samplers. The data are of sufficient detail so the three-dimensional movement of water and the two-dimensional movement of solute can be monitored.

Despite the large variations in saturated hydraulic conductivities reported by *Wierenga et al.* [1989, this issue] for the Las Cruces Trench Site, the movement of water and bromide during the first 71 days of infiltration appears to be fairly homogeneous. In contrast, highly concentrated areas of tritium exist on one side of the irrigated area on day 71. After 201 days of redistribution there appears to be little motion of tritium, but significant heterogeneous motion of bromide. The water in the plane nearest to the solute samplers also moves in a similarly heterogeneous fashion during redistribution. In all cases, the leading edge of the solute front moves much slower than the leading edge of the water front due to the displacement of initial water in the soil profile. The effects of spatial variability on water flow appear to be more dominant in the y = 2 m plane than in the y = 6 m and 10 m planes. Because of this, it is not clear whether solute transport in the y = 6 m and 10 m planes would show a similarly heterogeneous behavior.

To test the completeness of the experimental results for modeling, a simple uniform soil, two-dimensional model for water flow and transport was implemented. Comparisons between the predicted changes in water content and the measured changes in water content show qualitative agreement for the vertical movement of the leading edge of the water plume after 71 days of infiltration for all three neutron probe planes. In contrast, qualitative comparisons between the observed and predicted plume widths for the three measurement planes show less satisfactory agreement and show an increased sensitivity to the effect of spatial variability. After 200 days of redistribution, fair agreement in the overall plume motion is demonstrated in the y = 6 m and 10 m planes but poor agreement is shown in the y = 2 m plane. Comparisons between the predicted and observed behavior of tritium and bromide show less satisfactory results. Model predictions of bromide transport were better during the initial 71 days of infiltration than they were after 200 days of redistribution. Model predictions for the motion of tritium were generally poor. As for the case of water flow, the increased effect of the spatial variability near the trench face during redistribution appears to be the primary reason for

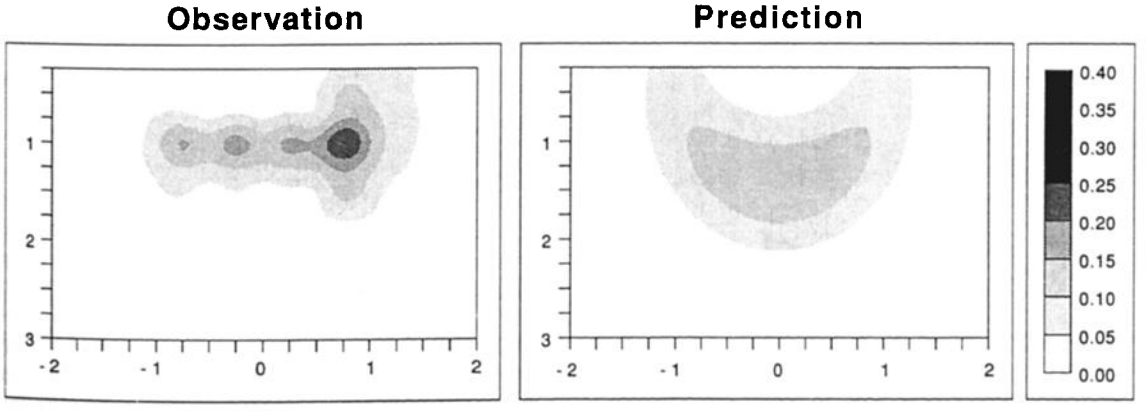

Fig. 12. Observed and predicted relative tritium concentrations on day 277: y = 0.5 m.

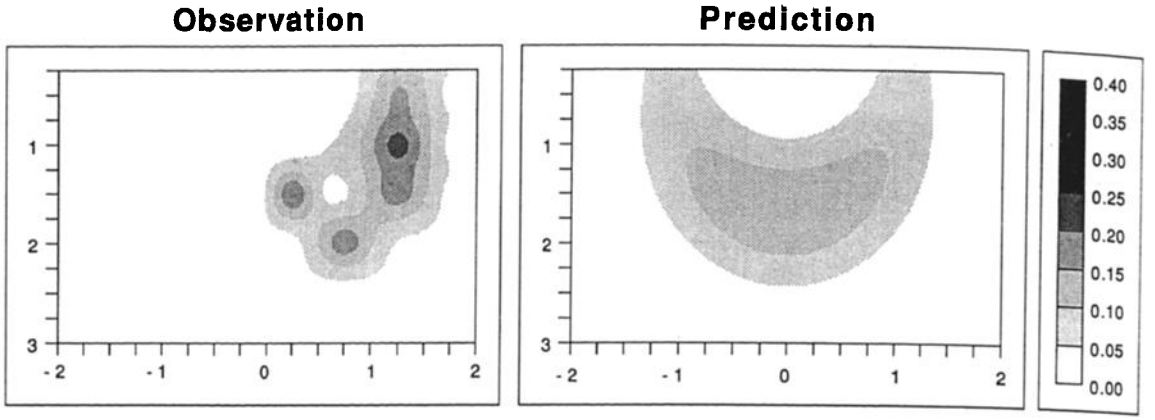

Fig. 13. Observed and predicted relative bromide concentrations on day 277: $y = 0.5$ m.

the larger discrepancies between predicted and observed solute movement.

APPENDIX

The following noniterative alternating direction implicit finite difference approximation is used to solve for water contents at time t^{n+1} given the water contents at time t^n (see (2)):

$$\frac{\theta^*_{i,k} - \theta^n_{i,k}}{\Delta t/2} = \frac{1}{\Delta x}\left(D^n_{i+1/2,k}\frac{\theta^n_{i+1,k} - \theta^n_{i,k}}{\Delta x} - D^n_{i-1/2,k}\frac{\theta^n_{i,k} - \theta^n_{i-1,k}}{\Delta x}\right) + \frac{1}{\Delta z}\left(D^n_{i,k+1/2}\frac{\theta^*_{i,k+1} - \theta^*_{i,k}}{\Delta z} - D^n_{i,k-1/2}\frac{\theta^*_{i,k} - \theta^*_{i,k-1}}{\Delta z}\right) - \frac{K^n_{i,k+1/2} - K^n_{i,k-1/2}}{\Delta z} \quad \text{(A1)}$$

for the first half of the time step and

$$\frac{\theta^{n+1}_{i,k} - \theta^*_{i,k}}{\Delta t/2} = \frac{1}{\Delta x}\left(D^n_{i+1/2,k}\frac{\theta^{n+1}_{i+1,k} - \theta^{n+1}_{i,k}}{\Delta x} - D^n_{i-1/2,k}\frac{\theta^{n+1}_{i,k} - \theta^{n+1}_{i-1,k}}{\Delta x}\right) + \frac{1}{\Delta z}\left(D^n_{i,k+1/2}\frac{\theta^*_{i,k+1} - \theta^*_{i,k}}{\Delta z} - D^n_{i,k-1/2}\frac{\theta^*_{i,k} - \theta^*_{i,k-1}}{\Delta z}\right) - \frac{K^n_{i,k+1/2} - K^n_{i,k-1/2}}{\Delta z} \quad \text{(A2)}$$

for the second half of the time step. In the above equations, i and k represent the node number in the x and z directions, respectively. The grid points are centered in each of the mesh grid volumes. The nodes represent volume averages rather than intersections of the grid mesh. This nodal scheme simplifies the numerical conservation of mass. The intergrid values for the properties are given by simple averages, i.e.,

$$D^n_{i+1/2,k} = \frac{D^n_{i+1,k} + D^n_{i,k}}{2} \quad \text{(A3)}$$

$$D^n_{i,k+1/2} = \frac{D^n_{i,k+1} + D^n_{i,k}}{2} \quad \text{(A4)}$$

$$K^n_{i,k+1/2} = \frac{K^n_{i,k+1} + K^n_{i,k}}{2} \quad \text{(A5)}$$

Note that the use of (A5) in (A1) and (A2) is equivalent to using center differences for the gravity-induced convective term. Note also that the properties are evaluated at the old time step and no subiterations are performed. A tridiagonal solver is used during each half time step to first solve implicitly for the $\theta^*_{i,k}$ along the y direction and then for the $\theta^{n+1}_{i,k}$ along the x direction. Flux boundary conditions are modeled in the usual fashion through the use of imaginary nodes so that second-order accuracy can be maintained. After the water content is updated to the next time step, the Darcian fluxes are evaluated using

$$q^*_{x_{i+1/2,k}} = -D^n_{i+1/2,k}\frac{\theta^n_{i+1,k} - \theta^n_{i,k} + \theta^{n+1}_{i+1,k} - \theta^{n+1}_{i,k}}{2\Delta x} \quad \text{(A6)}$$

$$q^*_{z_{i,k+1/2}} = K^n_{i,k+1/2} - D^n_{i,k+1/2}\frac{\theta^*_{i,k+1} - \theta^*_{i,k}}{\Delta x} \quad \text{(A7)}$$

Note that the x direction fluxes are evaluated using an average of the n and the $n + 1$ time step fluxes whereas the z direction fluxes use the intermediate time step fluxes. Evaluating fluxes in this fashion is required if the water fluxes used in the solute transport equation are to be equivalent to the water transported as calculated from (A1) and (A2). Once the water fluxes are evaluated, the solute transport (see (8)) is updated by the following alternating direction implicit scheme:

$$R\frac{\theta^*_{i,k}c^*_{i,k}-\theta^n_{i,k}c^n_{i,k}}{\Delta t/2}=\frac{1}{\Delta x}\left((\theta^*_{i+1/2,k}D^n_{s_{i+1/2,k}})\frac{c^n_{i+1,k}-c^n_{i,k}}{\Delta x}\right.$$
$$\left.-(\theta^*_{i-1/2,k}D^n_{s_{i-1/2,k}})\frac{c^n_{i,k}-c^n_{i-1,k}}{\Delta x}\right)$$
$$-\frac{q^*_{x_{i+1/2,k}}c^n_{i+1/2,k}-q^*_{x_{i-1/2,k}}c^n_{i-1/2,k}}{\Delta x}$$
$$+\frac{1}{\Delta z}\left((\theta^*_{i,k+1/2}D^n_{s_{i,k+1/2}})\frac{c^*_{i,k+1}-c^*_{i,k}}{\Delta z}\right.$$
$$\left.-(\theta^*_{i,k-1/2}D^n_{s_{i,k-1/2}})\frac{c^*_{i,k}-c^*_{i,k-1}}{\Delta z}\right)$$
$$-\frac{q^*_{z_{i,k+1/2}}c^n_{i,k+1/2}-q^*_{z_{i,k-1/2}}c^n_{i,k-1/2}}{\Delta z} \quad \text{(A8)}$$

for the first half of the time step and

$$R\frac{\theta^{n+1}_{i,k}c^{n+1}_{i,k}-\theta^*_{i,k}c^*_{i,k}}{\Delta t/2}$$
$$=\frac{1}{\Delta x}\left((\theta^*_{i+1/2,k}D^n_{s_{i+1/2,k}})\frac{c^{n+1}_{i+1,k}-c^{n+1}_{i,k}}{\Delta x}\right.$$
$$\left.-(\theta^*_{i-1/2,k}D^n_{s_{i-1/2,k}})\frac{c^{n+1}_{i,k}-c^{n+1}_{i-1,k}}{\Delta x}\right)$$
$$-\frac{q^*_{x_{i+1/2,k}}c^n_{i+1/2,k}-q^*_{x_{i-1/2,k}}c^n_{i-1/2,k}}{\Delta x}$$
$$+\frac{1}{\Delta z}\left((\theta^*_{i,k+1/2}D^n_{s_{i,k+1/2}})\frac{c^*_{i,k+1}-c^*_{i,k}}{\Delta z}\right.$$
$$\left.-(\theta^*_{i,k-1/2}D^n_{s_{i,k-1/2}})\frac{c^*_{i,k}-c^*_{i,k-1}}{\Delta z}\right)$$
$$-\frac{q^*_{z_{i,k+1/2}}c^n_{i,k+1/2}-q^*_{z_{i,k-1/2}}c^n_{i,k-1/2}}{\Delta z} \quad \text{(A9)}$$

for the second half of the time step where

$$\theta^*_{i+1/2,k}=\frac{\theta^*_{i+1,k}+\theta^*_{i,k}}{2} \quad \text{(A10)}$$

$$\theta^*_{i,k+1/2}=\frac{\theta^*_{i,k+1}+\theta^*_{i,k}}{2} \quad \text{(A11)}$$

$$c^n_{i+1/2,k}=\frac{c^n_{i+1,k}+c^n_{i,k}}{2} \quad \text{(A12)}$$

$$c^n_{i,k+1/2}=\frac{c^n_{i,k+1}+c^n_{i,k}}{2} \quad \text{(A13)}$$

The water content–dispersion coefficient product is evaluated using

$$\theta^*_{i+1/2,k}D^n_{s_{i+1/2,k}}=\theta^*_{i+1/2,k}D_m+\varepsilon|\mathbf{q}^*_{i+1/2,k}| \quad \text{(A14)}$$

$$\theta^*_{i,k+1/2}D^n_{s_{i,k+1/2}}=\theta^*_{i+1/2,k}D_m+\varepsilon|\mathbf{q}^*_{i,k+1/2}| \quad \text{(A15)}$$

where

$$|\mathbf{q}^*_{i+1/2,k}|=\{(q^*_{x_{i+1/2,k}})^2+[(q^*_{z_{i+1,k+1/2}}+q^*_{z_{i,k+1/2}}+q^*_{z_{i+1,k-1/2}}+q^*_{z_{i,k-1/2}})/4]^2\}^{1/2} \quad \text{(A16)}$$

$$|\mathbf{q}^*_{i,k+1/2}|=\{[(q^*_{x_{i+1/2,k+1}}+q^*_{x_{i-1/2,k+1}}+q^*_{x_{i+1/2,k}}+q^*_{x_{i-1/2,k}})/4]^2+(q^*_{z_{i,k+1/2}})^2\}^{1/2} \quad \text{(A17)}$$

As for the finite difference approximation to Richards' equation, the boundary fluxes on solutes are implemented through the use of imaginary nodes to preserve second-order accuracy on the finite difference approximations.

Acknowledgments. The authors wish to acknowledge the support from the U.S. Nuclear Regulatory Commission and the U.S. Environmental Protection Agency. The advice of Lynn Gelhar and Dennis McLaughlin from the Massachusetts Institute of Technology, Glendon Gee from Battelle Pacific Northwest Laboratories, and Tom Nicholson of the U.S. Nuclear Regulatory Commission with the design and execution of the experiment is gratefully acknowledged. Finally, this project could not have been done without the help of Warren Strong, Joe Vinson, Jim Bilskie, Hesham Elabd, Mohammed Nash, Allan Schneeberger, Indrek Porro and Alex Toorman.

REFERENCES

Ababou, R., and L. W. Gelhar, A high-resolution finite difference simulator for 3D unsaturated flow in heterogeneous media, in *Computational Methods in Water Resources, Comput. Mech. Publ.*, vol. 1, pp. 173–178, Elsevier, Amsterdam, 1988.

Allen, M. B., and C. L. Murphy, A finite-element collocation method for variably saturated flow in two space dimensions, *Water Resour. Res.*, *22*(11), 1537–1542, 1986.

Hills, R. G., I. Porro, D. B. Hudson, and P. J. Wierenga, Modeling one-dimensional infiltration into very dry soils, 1, Model development and evaluation, *Water Resour. Res.*, *25*(6), 1259–1269, 1989*a*.

Hills, R. G., D. B. Hudson, I. Porro, and P. J. Wierenga, Modeling one-dimensional infiltration into very dry soils, 2, Estimation of the soil water parameters and model predictions, *Water Resour. Res.*, *25*(6), 1271–1282, 1989*b*.

Huyakorn, P. S., and G. F. Pinder, *Computational Methods in Subsurface Flow*, Academic, San Diego, Calif., 1983.

Huyakorn, P. S., B. G. Jones, and P. F. Andersen, Finite element algorithms for simulating three-dimensional groundwater flow and solute transport in multilayer systems, *Water Resour. Res.*, *22*(3), 361–374, 1986*a*.

Huyakorn, P. S., E. P. Springer, V. Guvanasen, and T. D. Wadsworth, A three-dimensional finite-element model for simulating water flow in variably saturated porous media, *Water Resour. Res.*, *22*(13), 1790–1808, 1986*b*.

Huyakorn, P. S., J. B. Kool, and J. B. Robertson, VAM2D—Variably saturated analysis model in two dimensions, *Rep. NUREG/CR-5352*, U.S. Nucl. Regul. Comm., Washington, D. C., 1989.

Kaluarachchi, J. J., and J. C. Parker, Finite element analysis of water flow in variably saturated soil, *J. Hydrol.*, *90*, 269–291, 1987.

Nielsen, D. R., M. T. van Genuchten, and J. W. Biggar, Water flow and solute transport processes in the unsaturated zone, *Water Resour. Res.*, *22*(9), 89S–108S, 1986.

van Genuchten, M. T., Calculating the unsaturated hydraulic conductivity with a new closed-form analytical model, *Rep. 78-WR-08*, Dep. of Civ. Eng., Princeton Univ., Princeton, N. J., 1980.

van Genuchten, M. T., A comparison of numerical solutions of the one-dimensional unsaturated-saturated flow and mass transport equations, *Adv. Water Resour.*, *5*, 47–55, 1982.

van Genuchten, M. T., An Hermitian finite element solution of the two-dimensional saturated-unsaturated flow equation, *Adv. Water Resour.*, *6*, 106–111, 1983.

Wierenga, P. J., D. Bachelet, J. R. Bilskie, H. Elabd, D. B. Hudson, M. Nash, I. Porro, W. R. Strong, A. Toorman, and J. Vinson, Validation of stochastic flow and transport models for unsaturated soils, *Res. Rep. 88-SS-03*, Dep. of Agron. and Hort., N. M. State Univ., Las Cruces, 1988.

Wierenga, P. J., A. F. Toorman, D. B. Hudson, J. Vinson, M. Nash, and R. G. Hills, Soil physical properties at the Las Cruces trench site, *Rep. NUREG/CR-5441*, U.S. Nucl. Regul. Comm., Washington, D. C., 1989.

Wierenga, P. J., R. G. Hills, and D. B. Hudson, The Las Cruces Trench Site: Characterization, experimental results, and one-dimensional flow predictions, *Water Resour. Res.*, this issue.

R. G. Hills and M. R. Kirkland, Mechanical Engineering Department, New Mexico State University, Las Cruces, NM 88003.

D. B. Hudson and P. J. Wierenga, Department of Soil and Water Science, University of Arizona, Tucson, AZ 85721.

(Received February 20, 1990;
revised May 22, 1991;
accepted June 10, 1991.)